The properties of a-SiGe:H films fabricated by a novel deposition method



2001 J. Phys.: Condens. Matter 13 6615

(http://iopscience.iop.org/0953-8984/13/31/303)

INSTITUTE OF PHYSICS PUBLISHING JOURNAL OF PHYSICS: CONDENSED MATTER

J. Phys.: Condens. Matter **13** (2001) 6615–6624 PII: S0953-8984(01)20909-6

# The properties of a-SiGe:H films fabricated by a novel deposition method

**B G Budaguan**[1], **A A Sherchenkov**[1], **G L Gorbulin**[1] **and V D Chernomordic**[2]

[1] Institute of Electronic Technology, Moscow 103498, Russia
[2] Institute of Microelectronics of the Russian Academy of Science, Yaroslavl 150007, Russia

E-mail: budaguan@ms.miee.ru

Received 15 January 2001, in final form 1 June 2001
Published 19 July 2001
Online at stacks.iop.org/JPhysCM/13/6615

**Abstract**

In this work a novel 55 kHz plasma-enhanced chemical vapour deposition (PECVD) technique for deposition of a-SiGe:H films at high deposition rates is developed. According to infrared spectroscopy and atomic force microscopy analysis the 55 kHz a-SiGe:H films possess island-type microstructure. The Si–$H_n$ and Ge–$H_n$ configurations are clustered on the island surfaces and do not affect the optical band gap. The Tauc band gap is determined by the concentration of Ge–Si bonds formed in the interior of the islands. At low germanium content in the gas mixture ($R_{Ge} \leqslant 27.5\%$) the Si–$H_n$-related microstructure controls the Fermi level position while the formation of Ge-related defects determines which recombination centres are formed in the a-SiGe:H films. At $R_{Ge} > 27.5\%$ the formation of Ge–$H_n$ microstructure controls the optoelectronic properties of 55 kHz PECVD a-SiGe:H films.

## 1. Introduction

Amorphous hydrogenated silicon (a-Si:H) and its alloys are widely used in the fabrication of optoelectronic devices such as photodetectors, sensors and solar cells. Traditionally, p–i–n structures are used for the formation of solar cells on the basis of a-Si:H. In such devices, a thick undoped i-layer is necessary for the absorption of light and generation of charge carriers. In this case, charge carriers are generated only by photons with energies higher than the band gap of the i-type a-Si:H. In order to overcome this drawback, solar cells with two and more p–i–n structures, incorporating undoped amorphous materials with different band gaps, must be fabricated. In such stacked solar cells light first passes through the p–i–n structure with higher-band-gap material and then through that with lower-band-gap material. As a result, tandem and triplet solar cells allow one to increase the efficiency of the utilization of the solar spectrum and increase the stabilized efficiency of these electronic devices.

Usually a-SiGe:H alloys are used as the low-band-gap optoelectronic materials in tandem and triplet solar cells. However, the incorporation of Ge in a-Si:H increases the defect density

  

[1] and leads to deterioration of the optoelectronic properties of the alloy [2–4]. The high degree of hydrogen dilution of the gas mixture during the deposition procedure improves the properties of a-SiGe:H [5, 6]. However, this significantly decreases the deposition rate [7, 8]. Increase of the deposition rate of the active photoconductive layer is necessary to reduce the degradation of the previously fabricated layers during the deposition, and to enhance the cost/efficiency ratio, which is an important factor for industrial implementation of solar cell technology.

In this work a 55 kHz PECVD method is applied to achieve a high rate of fabrication of photoconductive a-SiGe:H films. Previously [4, 9], this method was successfully used to achieve a high rate of deposition of a-Si:H films with properties suitable for solar cell fabrication.

## 2. Experiment

The a-SiGe:H films were fabricated by 55 kHz PECVD [4] on c-Si and Corning 7059 glass substrates at different $GeH_4$ contents in a gas mixture with $R_{Ge} = 100[GeH_4]/[SiH_4+GeH_4]\%$. The deposition was performed in a quartz tube reactor 230 mm in diameter and 800 mm in length (figure 1). The gases entered the reactor through the inlet in the front part, flowed between the electrodes and were pumped out through the outlet in the rear part of the reactor by a two-step backing pump. The pressure in the reactor was controlled using a throttle valve placed between the outlet and the pump. The substrates were installed on four parallel-plate graphite electrodes, $180 \times 360$ mm, which were placed axially to the gas flow (the interelectrode gap was 14 mm). The temperature of the substrates was controlled by an external resistive heater, which was coaxial with the quartz reactor. Electrodes were connected such that three symmetrical discharges were created, and every electrode played the role of a cathode during one half-period, and the role of an anode during the other half-period. In this electrode system the gas decomposition regions are close to the substrates [9], which leads to a higher deposition rate for a-Si:H films (1–2.5 nm $s^{-1}$).

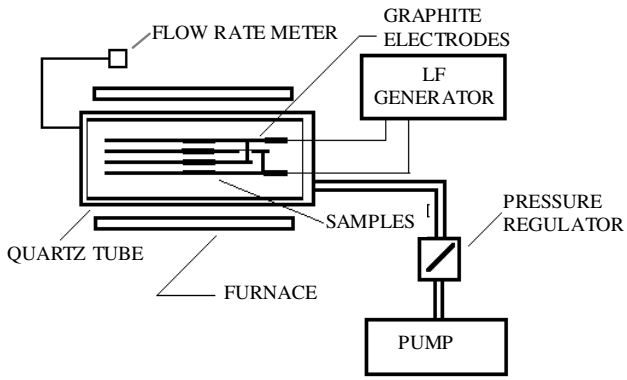


**Figure 1.** The scheme for the 55 kHz PECVD reactor.

The low-frequency (LF) power, the total gas pressure and the substrate temperature were kept at constant values of 150 W, 70 Pa and 225 °C, respectively. The film thicknesses were in the range from 0.64 to 0.90 $\mu$m.

The analysis of the chemical composition, concentration and distribution of hydrogen in a-SiGe:H films was carried out by means of measurements of infrared (IR) transmission spectra using a double-beam spectrometer (SPECORD M-80). The surface morphology of the

films was investigated by atomic force microscopy (AFM) with a scanning probe microscope P4-SPM-MDT [10].

The Tauc optical band gap, $E_g$, was estimated from measurements made on optical absorption spectra taken using a double-beam spectrophotometer (SPECORD-40) over the wavelength range of 300–900 nm [11]. The dark-photoconductivity measurements were carried out over the temperature range of 20–250 °C at a heating rate of 5 °C $min^{-1}$. The experimental set-up is shown in figure 2. For the photoconductivity measurements a He–Ne laser ($\lambda = 633$ nm) with an illumination intensity of $9.6 \times 10^{16}$ $cm^{-2}$ $s^{-1}$ was used. To avoid the degradation of samples during the illumination, the measurement times were kept below 3 s. To achieve this, a shield was used to prevent the laser beam from reaching the sample between the photoconductivity measurements.

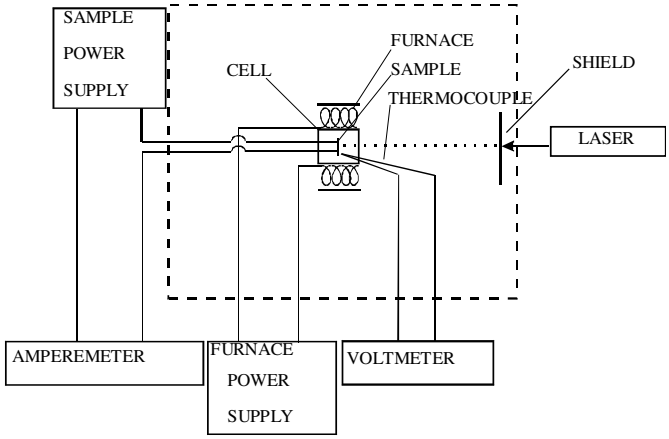


**Figure 2.** The scheme of the set-up for the photoconductivity measurements.

## 3. Results

The rates of deposition, $V_d$, of a-SiGe:H films fabricated by 55 kHz PECVD for different values of $R_{Ge}$ are presented in table 1. As is seen from the table 1, the growth rate of a-SiGe:H fabricated by the 55 kHz PECVD method is higher than the literature data (∼1–1.2 Å $s^{-1}$) [12]. Because the binding energy of Ge–H is lower in comparison with that of Si–H [13] it is assumed that decomposition of $SiH_4$ controls the growth rate for a-SiGe:H films. This growth mechanism is supported by the near independence of $V_d$ of the $GeH_4$ content. So, the high rate of deposition of a-SiGe:H in 55 kHz PECVD is caused by the same factor as in the case of a-Si:H [9], i.e. by an increased flux of radicals to the growth surface due to the closeness of the radical generation region to the electrodes.

Tauc plots for a-SiGe:H films deposited at different $R_{Ge}$-values are presented in figure 3. These plots were used for the calculation of the optical Tauc band gap, $E_g$, from the equation [14]

$$(\alpha h\nu)^{1/2} = B(h\nu - E_g)$$

where $\alpha$, $h\nu$ and $B$ are the optical absorption coefficient, photon energy and Tauc slope, respectively.

The dependence of the Tauc band gap on $R_{Ge}$ is presented in figure 4. It is seen that $E_g$ decreases with the increase of the germane ($GeH_4$) content in the gas mixture and hence with

**Table 1.** The deposition rate, $V_d$, the optical band gap, $E_g$, the ratio $\sigma_{ph}/\sigma_{d300}$, and the average diameter of islands, $D_{av}$, for a-SiGe:H films fabricated by 55 kHz PECVD at different $GeH_4$ contents, $R_{Ge}$.

| $R_{Ge}$ (%) | $V_d$ (Å $s^{-1}$) | $E_g$ (eV) | $\sigma_{ph}/\sigma_{d300}$ | $D_{av}$ (nm) |
|---|---|---|---|---|
| 0 | 11.1 | 1.70 | $9.35 \times 10^3$ | 81.5 |
| 9.1 | 8.9 | 1.63 | $5.93 \times 10^3$ | 88.4 |
| 16.7 | 12.5 | 1.54 | $4.84 \times 10^2$ | 89.8 |
| 27.5 | 12.5 | 1.37 | 9.58 | 97.8 |
| 37.5 | 9.4 | 1.31 | $1.78 \times 10^1$ | 107.9 |
| 44.5 | 11.4 | 1.25 | 2.57 | 106.4 |

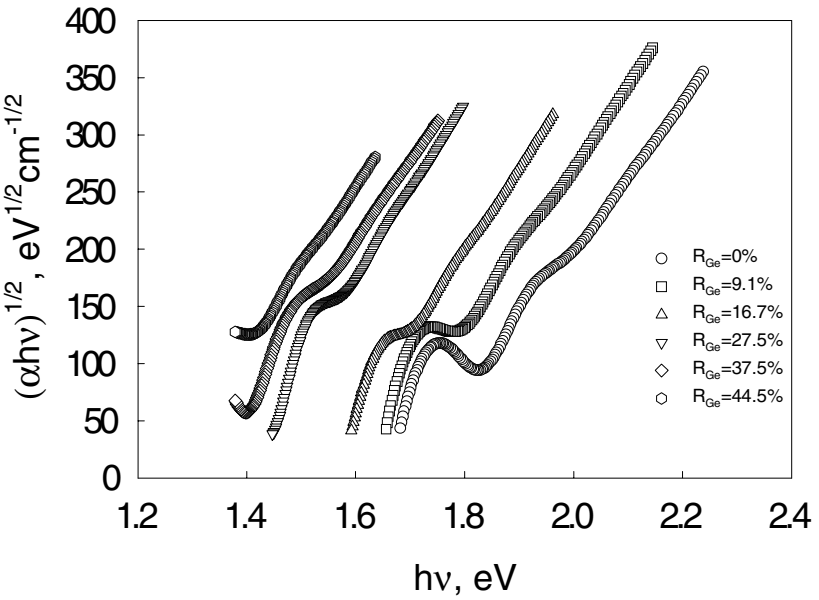


**Figure 3.** Tauc plots for 55 kHz a-SiGe:H films for different $R_{Ge}$-values.

the increase of the germanium content in the film. A linear relation between optical band gap and germanium content is usually reported in the literature [15, 16]. For our a-SiGe:H films a slight change in the slope is seen at $R_{Ge} = 27.5\%$.

Typical temperature dependencies of the dark conductivity, $\sigma_{d300}$, and of the photoconductivity, $\sigma_{ph}$, for a-SiGe:H fabricated at $R_{Ge} = 9.1\%$ are presented in figure 5. From these measurements the ratios $\sigma_{ph}/\sigma_{d300}$, at room temperature, for the samples fabricated at different $R_{Ge}$-values were determined (see table 1). The data obtained are in good agreement with the data of [7, 8].

From the temperature dependence of the dark conductivity, the activation energy, $E_a$, was determined from the equation

$$\sigma_d = \sigma_0 \exp[-E_a/kT]$$

where: $\sigma_d$ is the dark conductivity; $\sigma_0$ is the pre-exponential factor; $kT$ is the thermal energy.

According to the work [17] the conduction in a-SiGe:H films at temperatures above room temperature is determined by electrons excited above a mobility edge $E_C$. So, the Fermi level

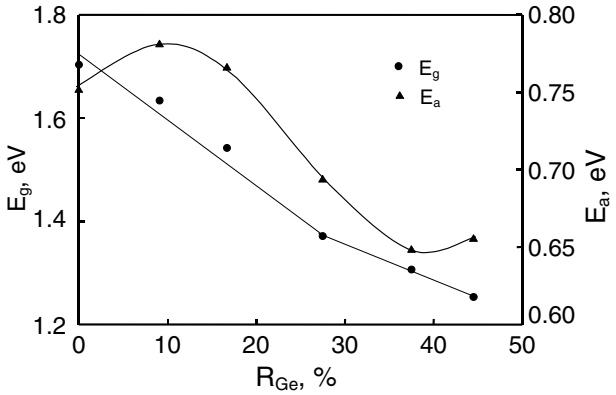


**Figure 4.** The dependencies of $E_g$ and $E_a$ for 55 kHz a-SiGe:H films on $R_{\mathrm{Ge}}$.

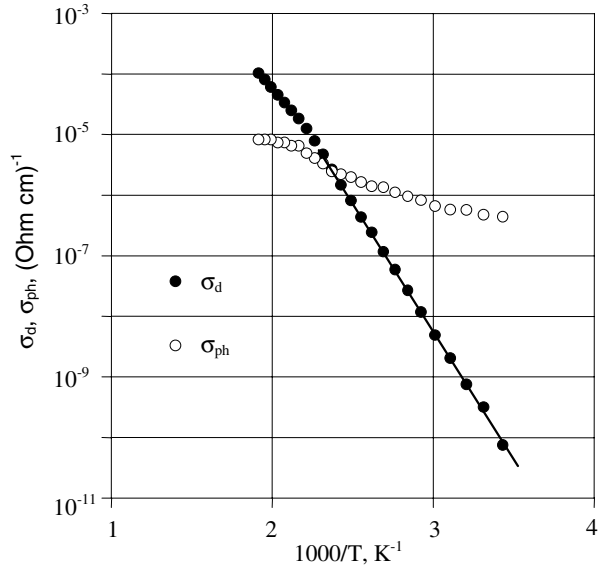


**Figure 5.** The temperature dependencies of the dark photoconductivity for a-SiGe:H film fabricated by 55 kHz PECVD at $R_{\mathrm{Ge}} = 9.1\%$.

position extrapolated to $T = 0$ K can be estimated from $E_a = (E_F - E_C)_0$, where $E_F$ is the Fermi energy level, $E_C$ is the conduction band edge.

The dependence of the dark-conductivity activation energy on the germane content in the gas mixture is presented in figure 4. It can be seen that at $R_{\mathrm{Ge}} = 9.1\%$ the activation energy increases while $E_g$ decreases, which indicates a shift of the Fermi level to the mid-gap. At higher germane content, $E_a$ decreases in accordance with the decrease of the Tauc band gap.

The results of the calculations of $E_g$ and $E_a$ were used for the analysis of the a-SiGe:H band diagram. The dependence of the energy band diagram on $R_{\mathrm{Ge}}$ is shown in figure 6. All energy levels are considered with respect to the middle of the band gap. Following the work [18], we suppose that $E_V$ and $E_C$ change symmetrically with respect to the mid-gap. In that case the Fermi level shifts to the valence band with the initial introduction of $GeH_4$ into the gas mixture and then locates near the mid-gap with the further increase of $R_{\mathrm{Ge}}$.

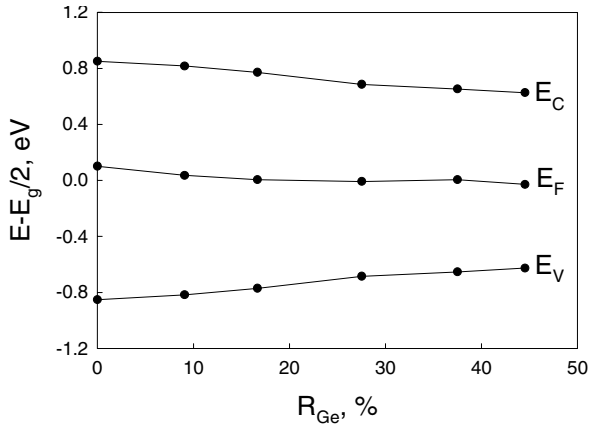


**Figure 6.** The band diagram of a-SiGe:H alloys fabricated by 55 kHz PECVD.

The composition and different bond configurations were investigated by IR spectroscopy analysis. The IR spectra of the a-SiGe:H films deposited at different $R_{Ge}$-values are presented in figure 7. The mixing of Si–H and Ge–H wagging vibrations was attributed to the integrated IR peak at 605–634 $cm^{-1}$ [19]. So, the intensity of this peak corresponds to the total hydrogen content. The Ge–H and Ge–$H_n$ stretching vibrations [20] were obtained by decomposition of the stretching band at 1866–1920 $cm^{-1}$ into two Gaussians with peaks at 1866–1892 $cm^{-1}$ and 1911–1922 $cm^{-1}$, respectively. In the same way, Si–H and Si–$H_n$ stretching peaks were obtained at 2000–2006 $cm^{-1}$ and 2042–2068 $cm^{-1}$, respectively [11]. It is seen from figure 7

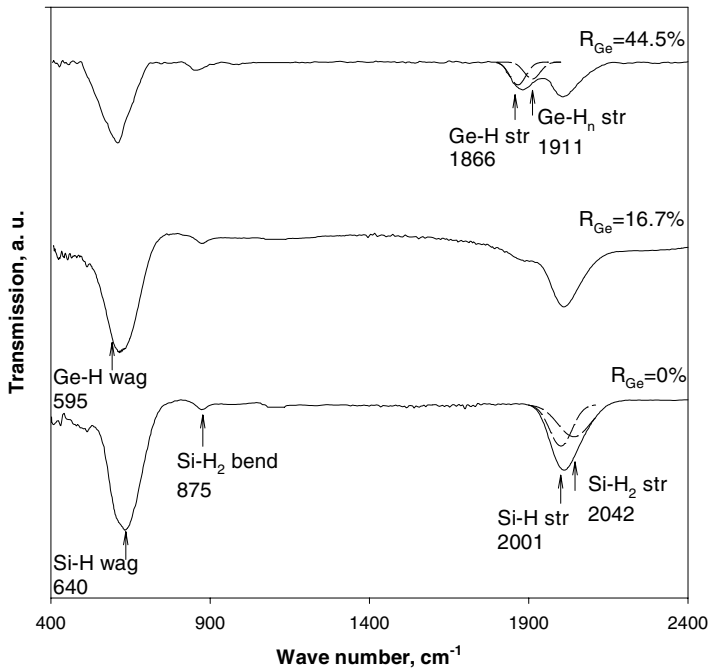


**Figure 7.** IR transmission spectra of 55 kHz a-SiGe:H film.

that at $R_{Ge} \geqslant 9.1\%$ the peak at 1866–1892 $cm^{-1}$ appears. This fact and the shift of the peak at 605–634 $cm^{-1}$ to lower wavenumbers are attributed to the formation of Ge–H bonds in the film. At $R_{Ge} > 37.5\%$ a shoulder at 1910–1920 $cm^{-1}$ was seen, indicating the formation of Ge-related microstructure.

The surface morphology of a-SiGe:H films was investigated by AFM analysis. The AFM image for the film deposited at $R_{Ge} = 9.1\%$ is presented in figure 8. The island-type microstructure was observed for all samples investigated and was observed previously in a-Si:H films [4, 10].

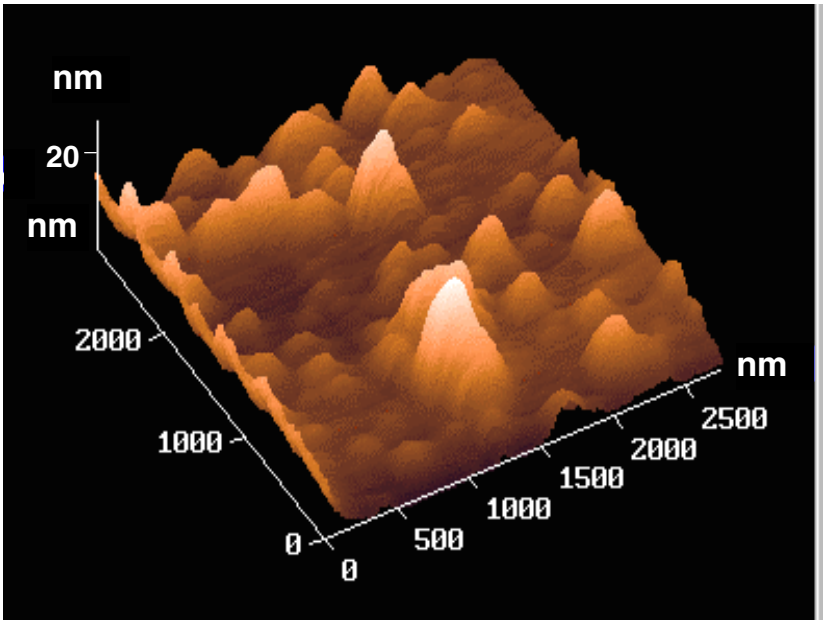


**Figure 8.** An AFM image of 55 kHz a-SiGe:H film at $R_{Ge} = 9.1\%$.
(This figure is in colour only in the electronic version)

The island size distribution was determined by calculation of the number of islands with different diameters, $D$, on the surface of a $2.5 \times 2.5\ \mu m^2$ area. Then histograms of the island diameter distributions were plotted (figure 9). For this purpose the diameter range from the lower value to the higher one was divided into parts and the proportions of the island diameters in per cent, $f$, which appeared in each part were determined. After that the histograms of the island diameter distributions were approximated by a log-normal distribution (see figure 9) [10]:

$$\Lambda(D) = \frac{1}{\sqrt{2\pi}\sigma D} \exp\left(-\frac{1}{2}\left(\frac{\ln(D/m)}{\sigma}\right)^2\right)$$

where $m$ and $\sigma$ are the median and the width (dimensionless) of the distribution on a logarithmic scale.

The average diameter of the islands, $D_{av}$, was determined according to the equation [10]

$$D_{av} = m \exp(\sigma^2/2).$$

The results of the calculations of $D_{av}$ are presented in table 1. It is seen from the table that the average diameter of the islands increases with the increase of $R_{Ge}$.

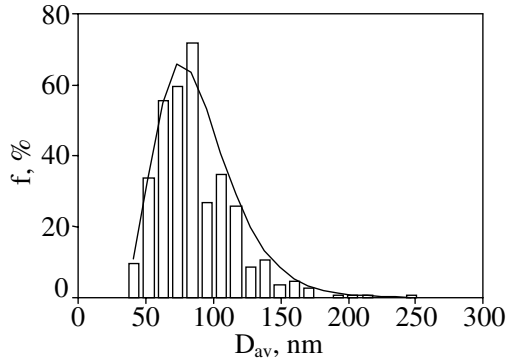


**Figure 9.** The histogram of the island size distribution for a-SiGe:H films deposited at $R_{Ge} = 16.7\%$. The solid line is the fitting curve for the experimental data.

## 4. Discussion

The dependencies of the dark conductivity, photoconductivity, and dark-conductivity activation energy on $E_g$ are presented in figure 10. The decrease of $E_g$ first leads to decreases of $\sigma_{d300}$ and $\sigma_{ph}$ and to a shift of the Fermi level to the middle of the band gap. At $E_g = 1.63$ eV the ratio of the photoconductivity to the dark conductivity at room temperature is the same as for a-Si:H films. This result reveals the highly photoconductive nature of low-band-gap a-SiGe:H films prepared at high deposition rates by 55 kHz PECVD. With further decrease of the Tauc optical band gap, $\sigma_{ph}$ is nearly independent of $E_g$ while $\sigma_{d300}$ increases in accordance with the decrease of the dark-conductivity activation energy.

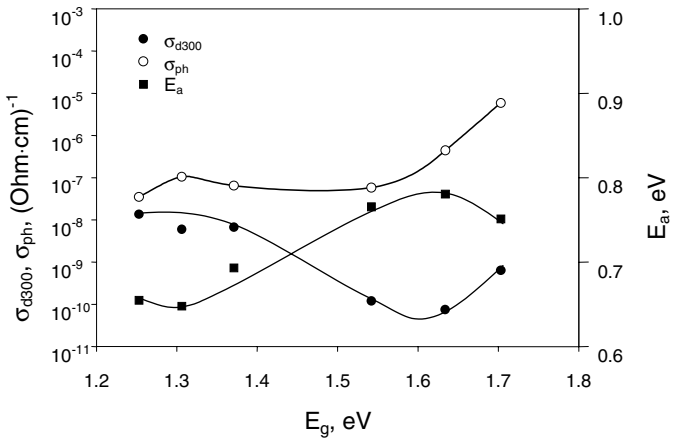


**Figure 10.** The dependencies of $\sigma_{d300}$, $\sigma_{ph}$ and $E_a$ on the optical band gap, $E_g$.

In an effort to understand the peculiarities of the optoelectronic properties of a-SiGe:H films fabricated by high-rate 55 kHz PECVD technology, an analysis of film microstructure was carried out.

The dependencies of the IR peak intensities corresponding to different bonding configurations on $GeH_4$ content in the gas mixture are shown in figure 11. According to the IR spectra, the $(Ge–H)_{str}$ peak intensity increases and that of $(Si–H)_{str}$ decreases with increase

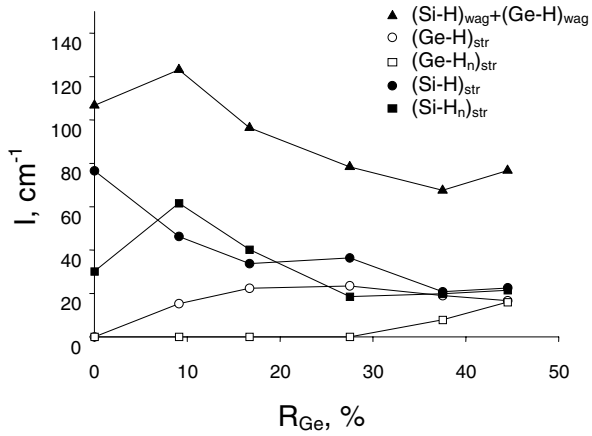


**Figure 11.** The dependencies of the IR peak intensities on $R_{Ge}$ for a-SiGe:H films.

of $R_{Ge}$ up to 27.5% . This means that adding $GeH_4$ to a gas mixture leads to substitution of Ge–H bonds for Si–H bonds. At the same time, in this composition range, the Si–$H_n$ bond configuration dominates and controls the total amount of hydrogen in the a-SiGe:H films. As is seen from figure 10, at $R_{Ge} \leqslant 27.5\%$ ($E_g \geqslant 1.37$ eV) the photoconductivity decreases with the increase of $R_{Ge}$. Taking into account the preferential attachment of H to Si [19–21], this means that in this composition range the recombination centres in a-SiGe:H films increase in number due to the formation of Ge-induced defects. On the other hand, the change of the dark-conductivity activation energy (see figure 4) is connected with the change of the total hydrogen content, particularly with Si–$H_n$ bonds. This means that Si–$H_n$-related microstructure controls the Fermi level position in a-SiGe:H films.

At $R_{Ge}$ higher than 27.5%, $(Ge–H_n)_{str}$ vibration corresponding to clustered Ge–H bonds appears and increases in intensity with the increase of the $GeH_4$ content. According to the optoelectronic data (see figure 10) a slight change in the slope of the dependence of the Tauc band gap on the $GeH_4$ content in the gas mixture is observed. Meanwhile, the photoconductivity remains constant while the dark conductivity increases and the activation energy decreases. So, in that compositional range the formation of Ge–$H_n$ microstructure controls the optoelectronic properties of 55 kHz PECVD a-SiGe:H films.

The AFM data showed (see table 1) that $D_{av}$ initially slightly increases with the increase of the $GeH_4$ content in the gas mixture, which is connected with substitution of Ge–H bonds for Si–H bonds (see figure 11). A more pronounced increase is observed when clustered Ge–$H_n$ bonds appear in IR spectra. The relation between the average island diameter and the intensity of the Ge–H and Ge–$H_n$ stretching vibrations means that Ge–H-related microstructure is responsible for the increase of the average diameter of islands on a-SiGe:H surfaces. It is suggested that Si–$H_n$ and Ge–$H_n$ configurations are clustered on the island surfaces. This is responsible for the independence of $E_g$ of the total hydrogen content for 55 kHz films. Therefore, the decrease of $E_g$ with the increase of $R_{Ge}$ is determined by the increase of the concentration of Ge–Si bonds formed in the interior of the islands.

## 5. Conclusions

A novel 55 kHz PECVD technique was developed for deposition of a-SiGe:H films at high deposition rates. According to IR spectroscopy and AFM data the a-SiGe:H films possess

island-type microstructure. The Si–$H_n$ and Ge–$H_n$ configurations are clustered on the island surfaces and do not affect the optical band gap. In this case the Tauc band gap is determined by the concentration of Ge–Si bonds formed in the interior of the islands. At $R_{Ge} \leqslant 27.5\%$ the Si–$H_n$-related microstructure controls the Fermi level position while the formation of Ge-related defects determines which recombination centres are formed in the a-SiGe:H films. At $R_{Ge} > 27.5\%$ the formation of Ge–$H_n$ microstructure controls the optoelectronic properties of 55 kHz PECVD a-SiGe:H films. It was shown that high photoconductivity was achieved for low-band-gap a-SiGe:H films with $E_g = 1.63$ eV.

## Acknowledgments

This work was supported by the Grants from the Ministry of Education of the Russian Federation 107-GB-53-B-MFH, 259-GB-53-Gr-MFH, 269-GB-53-Gr-MFH, and the NATO Collaborative Research Grant PST.CLG 975481.

## References

[1] Palinginis K C, Cohen J D, Yang J C and Guha S 2000 *J. Non-Cryst. Solids* **266–269** 665
[2] Mackenzie K D, Burnett J H, Eggert J R, Li Y M and Paul W 1988 *Phys. Rev.* B **38** 6120
[3] Chen L, Tauc J, Lee J-K and Schiff E A 1991 *Phys. Rev.* B **43** 11 694
[4] Budaguan B G, Sherchenkov A A, Stryahilev D A, Sazonov A Yu, Radoselsky A G, Chernomordic V D, Popov A A and Metselaar J W 1998 *Electrochem. Soc.* **145** 2508
[5] Matsuda A and Tanaka K 1987 *J. Non-Cryst. Solids* **97+98** 1367
[6] Shima M, Terakawa A, Isomura M, Haku H, Tanaka M, Wakisaka K, Kiyama S and Tsuda S 1997 *17th Int. Conf. on Amorphous and Microcrystalline Semiconductors (Budapest, Hungary, 25–29 August 1997)*
[7] Rashad A, Sali J V, Marathe B R, Takwale M G and Shaligram A D 1999 *Solar Energy Mater. Solar Cells* **34** 209
[8] Dalal V L, Haroon S, Zhou Z, Maxson T and Han K 2000 *J. Non-Cryst. Solids* **266–269** 675
[9] Budaguan B G, Aivazov A A, Yu A Sazonov, Popov A A and Berdnikov A E 1997 *Mater. Res. Soc. Symp. Proc.* **467** 585
[10] Budaguan B G and Aivazov A A 1998 *Mater. Res. Soc. Symp. Proc.* **513** 387
[11] Budaguan B G, Aivazov A A, Stryahilev D A, Sokolov E M and Metselaar J W 1998 *J. Non-Cryst. Solids* **226** 217
[12] Kleider J P, Longeaud C, Roca i Cabarrocas P, St'ahel P and Sladek P *Proc. 2nd World Conf. on Photovoltaic Solar Energy Conversion (Vienna, July 1998)* pp 838–41
[13] Valladares A A, Valladares A and McNelis M A 1998 *J. Non-Cryst. Solids* **226** 67
[14] Tauc J, Grogorovici R and Vancu A 1966 *Phys. Status Solidi* **15** 627
[15] Wickbolt P, Pang D, Paul W, Chen J H, Zhong F, Chen C-C, Cohen J D and Williamson D L 1997 *J. Appl. Phys.* **81** 6252
[16] Folsch J, Finger F, Kulessa T, Siebke F, Beyer W and Wagner H 1995 *Mater. Res. Soc. Symp. Proc.* **377** 517
[17] Meaudre R, Meaudre M and Chanel J 1991 *Phys. Rev.* B **43** 9792
[18] Mackenzie K D, Eggert J R, Leopold D J, Li Y M, Lin S and Paul W 1985 *Phys. Rev.* B **31** 2198
[19] Chou Y-P and Lee S-C 1998 *J. Appl. Phys.* **83** 4111
[20] Terakawa A and Matsunami H 1999 *Japan. J. Appl. Phys.* **38** 6207
[21] Nelson B P, Xu Y, Webb J D, Mason A, Reedy R C, Gedvilas L M and Lanford W A 2000 *J. Non-Cryst. Solids* **266–269** 680